THE ASTROPHYSICAL JOURNAL, 473:L00-L00, 1996 December 20

HUBBLE SPACE TELESCOPE SPECTROSCOPIC EVIDENCE FOR A 1×10^9-$M_\odot$ BLACK HOLE IN NGC 4594[1]

JOHN KORMENDY,[2,3] RALF BENDER,[4] EDWARD A. AJHAR,[5] ALAN DRESSLER,[6] S. M. FABER,[7] KARL GEBHARDT,[8] CARL GRILLMAIR,[9] TOD R. LAUER,[5] DOUGLAS RICHSTONE,[8] AND SCOTT TREMAINE[10]

Received 1996 June 24; accepted 1996, September 24

ABSTRACT

The discovery by Kormendy of a $M_\bullet \simeq 10^9$ $M_\odot$ massive dark object (MDO) in NGC 4594 is confirmed with higher-resolution spectroscopy from the Canada-France-Hawaii Telescope (CFHT) and the *Hubble Space Telescope* (*HST*). CFHT measurements with the Subarcsecond Imaging Spectrograph improve the resolution from $\sigma_* = 0\farcs40$ to $0\farcs27$ Gaussian dispersion radius of the PSF. The apparent central velocity dispersion rises from $\sigma = 250 \pm 7$ km s^{-1} to 286 ± 7 km s^{-1}. As observed with the COSTAR-corrected *HST*, the Faint Object Spectrograph, and a $0\farcs21$ aperture, $\sigma = 321 \pm 7$ km s^{-1} is still higher, and the central rotation curve is very steep. The highest-$M_\bullet$ published dynamical model fits the new observations reasonably well when "observed" at *HST* resolution. The spatial resolution has now improved by a factor of ~ 5 since the discovery measurements, and the case for a black hole has strengthened correspondingly.

We confirm that NGC 4594 has a Seyfert spectrum; Hα is ~ 5200 km s^{-1} wide at zero intensity. However, gas velocities are lower than the circular velocities implied by the stars; they cannot be used to test the black hole case in NGC 4594. The gas may be in a ring, or it may be associated with patchy dust. *HST* images with the Second Wide Field and Planetary Camera show dust at some aperture positions.

NGC 4594 appears to have a bright point nucleus. However, the central absorption -ine strengths are low, consistent with dilution by enough nonthermal light to explain the "nucleus". There is no evidence for a distinct nuclear star cluster. NGC 4594 is similar to M 87, which also has a nonthermal nuclear source, and not to M 31 and NGC 3115, which have quiescent black holes and nuclear star clusters.

Subject headings: black hole physics – galaxies: individual (NGC 4594) – galaxies: kinematics and dynamics – galaxies: nuclei

1. INTRODUCTION

The COSTAR-corrected *Hubble Space Telescope* (*HST*) is spearheading a new and productive phase in the search for black holes (BHs) in galactic nuclei (see Kormendy & Richstone 1995 for a review). The first galaxy examined via stellar dynamics, NGC 3115, proved to have the largest velocity dispersion seen in any galactic nucleus, $\sigma = 600 \pm 37$ km s^{-1} (Kormendy *et al.* 1996, hereafter K+96). The ground-based MDO detection by Kormendy & Richstone (1992) was confirmed. Improved constraints on the radius inside which the dark mass lies also strengthened the conclusion that it is an $M_\bullet \simeq 2 \times 10^9$ $M_\odot$ BH.

This paper presents CFHT and *HST* spectroscopy of NGC 4594, the Sombrero Galaxy. Based on rapid rotation and a high central velocity dispersion observed with the CFHT at resolution $\sigma_* = 0\farcs40$, Kormendy (1988, hereafter K88) concluded that NGC 4594 contains a BH of mass $M_\bullet \simeq 10^9$ $M_\odot$. The kinematics are well confirmed (Jarvis & Dubath 1988; Wagner *et al.* 1989; Carter & Jenkins 1993; van der Marel *et al.* 1994; Emsellem *et al.* 1996) as is the dynamical analysis (Emsellem *et al.* 1994). But no paper has improved the spatial resolution. *HST* improves the resolution by a factor of 5. We show here that this greatly strengthens the BH case. More detailed dynamical models will then be presented in a later paper.

2. CFHT SIS SPECTROSCOPY

The CFHT Subarcsecond Imaging Spectrograph (SIS) was designed for problems like the BH search. The scale is $0\farcs0864$ pixel^{-1}; a slit width of $0\farcs26 \pm 0\farcs01$ was used. Tip-tilt guiding is incorporated; by offsetting the guide probe, we can center the object on the slit to one-pixel accuracy. An observing sequence consists of a series of direct images to center the object at the slit, an exposure with the slit in place but with no grism, the object spectrum, another image through the slit but without the grism and one with neither slit nor grism to verify that the object is still centered, and a comparison spectrum. The results in § 4 are based on the sum of two integrations totalling 70 min. The seeing was measured on the bracketing direct images. The brightness profile of the galaxy is the same in these images and in the spectrum, so the PSF in the images is correct for the spectrum. We obtain $\sigma_* = 0\farcs27 \pm 0\farcs01$ or FWHM $= 0\farcs63 \pm 0\farcs03$. This is a 33 % improvement over $\sigma_* = 0\farcs40$ in K88.

The spectra were taken near the Ca II infrared triplet, at 7975 – 8975 Å. The reciprocal dispersion was 0.98 Å pixel^{-1} = 34.6 km s^{-1} pixel^{-1}. The $2\farcm5$ slit was too short to let us measure the sky on galaxy spectra, so we used a summed sky spectrum taken from several exposures of

[1] Based on observations with the NASA/ESA *Hubble Space Telescope*, obtained at the Space Telescope Science Institute, which is operated by AURA, Inc., under NASA contract NAS 5-26555.

[2] Visiting Astronomer, Canada–France–Hawaii Telescope, operated by the National Research Council of Canada, the Centre National de la Recherche Scientifique of France, and the University of Hawaii.

[3] Institute for Astronomy, University of Hawaii, 2680 Woodlawn Dr., Honolulu, HI 96822.

[4] Universitäts-Sternwarte, Scheinerstraße 1, München 81679, Germany.

[5] Kitt Peak National Observatory, National Optical Astronomy Observatories, P. O. Box 26732, Tucson, AZ 85726.

[6] Carnegie Observatories, 813 Santa Barbara St., Pasadena, CA 91101.

[7] UCO/Lick Observatory, Univ. of California, Santa Cruz, CA 95064.

[8] Dept. of Astronomy, University of Michigan, Ann Arbor, MI 48109.

[9] Jet Propulsion Laboratory, Mail Stop 183-900, 4800 Oak Grove Drive, Pasadena, CA 91109.

[10] Canadian Institute for Theoretical Astrophysics, University of Toronto, 60 St. George Street, Toronto M5S 3H8, Canada.

small objects. This was scaled to the NGC 4594 spectra so that night sky emission lines subtracted as well as possible.

Velocities and velocity dispersions were calculated with the same Fourier quotient program that was used in K88. Results are averages for four standard stars, η Cyg (K0 III), κ Oph (K2 III), μ Leo (K2 III SMR), and γ Dra (K5 III).

3. *HST* FOS SPECTROSCOPY

NGC 4594 was observed on 1995 February 9 – 16 with the $0\farcs21$ square aperture and FOS. The aperture was placed along the disk major axis as shown in Figure 1. At radii $r = 0\farcs032$ W, $0\farcs163$ W, and $0\farcs207$ E, the integration times were 178, 228, and 228 min, respectively.

The spectra were electronically quarter-stepped, giving 2064, 1/4-diode pixels. Flat fielding and correction for geomagnetically induced motions were done as in K+96. The spectra were then resampled on a $\log\lambda$ scale at a reciprocal dispersion of 1.0837 Å pixel^{-1} = 58.3 km s^{-1} pixel^{-1}. The wavelength range, 4567 – 6800 Å over 2048 pixels, includes the Mg I b lines at $\lambda \simeq 5175$ Å and the Na I D lines at $\lambda \simeq 5892$ Å. The instrumental velocity dispersion was measured to be FWHM/2.35 = $\sigma_{\rm instr}$ = 1.77 ± 0.03 pixels = 103 ± 2 km s^{-1} (internal error). This is intrinsic to the instrument; it is not strongly affected by how the aperture is illuminated (Keyes *et al.* 1995). Therefore aperture illumination corrections to σ are small (see below).

Measured velocities depend on aperture illumination: if a star in the aperture is moved in the dispersion direction, V varies with position by 757 km s^{-1} arcsec^{-1}. The corrections for asymmetrical aperture illumination are larger here than they were for NGC 3115, because the major axis of NGC 4594 was oriented only $13\fdg2$ from the dispersion direction. We corrected for miscentering of the apertures on the galaxy using the final acquisition peakup intensity array. The apertures were placed at radii $0\farcs049$ W, $0\farcs162$ W, and $0\farcs204$ E of the center (Fig. 1). The luminosity-weighted mean radii are $0\farcs032$ W, $0\farcs163$ W, and $0\farcs207$ E, with estimated errors of about $\pm0\farcs003$.

Aperture corrections to V and σ were derived as follows. For each FOS spectrum, we divided the $0\farcs21$ aperture into 9 slices in the dispersion direction. We calculated the total brightness in each slice from our V-band WFPC2 image. We then velocity shifted the standard star spectrum appropriately for each slice, multiplied by the brightness in the slice, and added up the results. The sum divided by the total luminosity weight provides, for each aperture position, a standard star spectrum constructed such that the star and the galaxy illuminate the aperture in the same way. These star spectra were used to derive the kinematic results given below. Velocities and dispersions derived as above differ from those given by a standard star centered in the aperture by ≤ 12 km s^{-1} and ≤ 5 km s^{-1}, respectively.

The Mg b lines are contaminated with [NI] 5199 Å emission (Fig. 1). It is tempting to use the emission-free Na D lines to measure velocities. But Fig. 1 shows dust at some aperture positions. Also, the equivalent width of the D lines is a factor of 2 – 3 larger than in the comparison star. We conclude that Na D is contaminated by interstellar absorption. Therefore we measured the kinematics using Bender's (1990) Fourier correlation quotient program on a wavelength region (Fig. 1) that contains Mg b and Fe lines. We removed the emission line in two ways, (i) by interpolating through it, and (ii) by replacing the affected region iteratively with the broadened and velocity-shifted spectrum of NGC 3379 (Fig. 1). The two procedures give consistent results; $\sigma = 323 \pm 22$, 320 ± 11, and 312 ± 11 km s^{-1} at r = $0\farcs032$, $0\farcs163$, and $-0\farcs207$, respectively. However, the usable wavelength range is much reduced by the emission and interstellar absorption contamination. Therefore V and σ errors are larger than they were in K+96 and line-of-sight velocity distributions cannot be measured.

The *HST* and CFHT data are illustrated in Figure 2. The left panel includes measurements by van der Marel *et al.* (1994) that have much higher signal-to-noise ratios than our data. However, they do not well resolve the nuclear disk, so they are plotted only at $r > 12''$.

4. RESULTS: COMPARISON WITH K88 MODELS

The dynamical components of NGC 4594 show up well in Fig. 2 (*left*). NGC 4594 contains a nuclear disk of stars (Fig. 1; Burkhead 1986, 1991; K88; Emsellem *et al.* 1994, 1996) that is more prominent than the one in NGC 3115 (K+96). It affects the isophotes at $r \lesssim 8''$. At $10''$ – $15''$ radius along the major axis, the light is dominated by the bulge, and at still larger radii, the main disk takes over. These features are recognizable in the SIS data. At $r \gtrsim 30''$, the kinematics are dominated by the main disk: V is large and σ is small. Nearer the center, V decreases and σ increases as the bulge contribution increases. By $r \simeq 10''$ – $12''$, the kinematics are purely those of the bulge: σ equals the minor-axis bulge dispersion (K88). Then, at $r < 10''$, the kinematics become those of the nuclear disk. This is quite cold: at $r \simeq 4''$ – $6''$, σ is smaller than the bulge dispersion despite rotational line broadening. At $r \gtrsim 1''$, the rotation curve is resolved (see also Carter & Jenkins 1993). But at $r < 1''$, $V(r)$ and $\sigma(r)$ are so steep that they are unresolved. The rapid central rise in $V(r)$ and the central jump in $\sigma(r)$ are the signature of the MDO.

The MDO case is strengthened by the observation that, as resolution improves, the apparent central kinematic gradients get steeper. The *HST* data imply that the rotation velocity $V \simeq 110$ km s^{-1} already at $0\farcs14$ radius. Similarly, the velocity dispersion gradient gets steeper at better resolution; the apparent central velocity dispersion rises from $\sigma(0) = 250 \pm 7$ km s^{-1} in K88 to 286 ± 7 km s^{-1} in the SIS data and 321 ± 7 km s^{-1} in the *HST* data.

Testing the BH case requires comparison with dynamical models. Making new models is complicated because of the many components; we postpone it to a later paper. However, as in K+96, the BH case can already be checked by comparing published models with the new data.

K88 computed models of NGC 4594, each consisting of an unprojected rotation curve, a velocity dispersion profile, and a volume brightness profile. To prevent the results from being too affected by the composite (hot + cold) stellar population (i. e., by non-Gaussian line-of-sight velocity distributions), the bulge spectrum was subtracted and the nuclear disk was modeled. This removed most of the two-component structure in the line profiles that has been emphasized by van der Marel *et al.* (1994) and by Emsellem *et al.* (1996). The residual line profiles were well fitted by the models (Kormendy 1994). Eleven models were constructed; they differed mainly in the steepness of their central kinematic gradients and in their maximum V and σ values. They bracketed

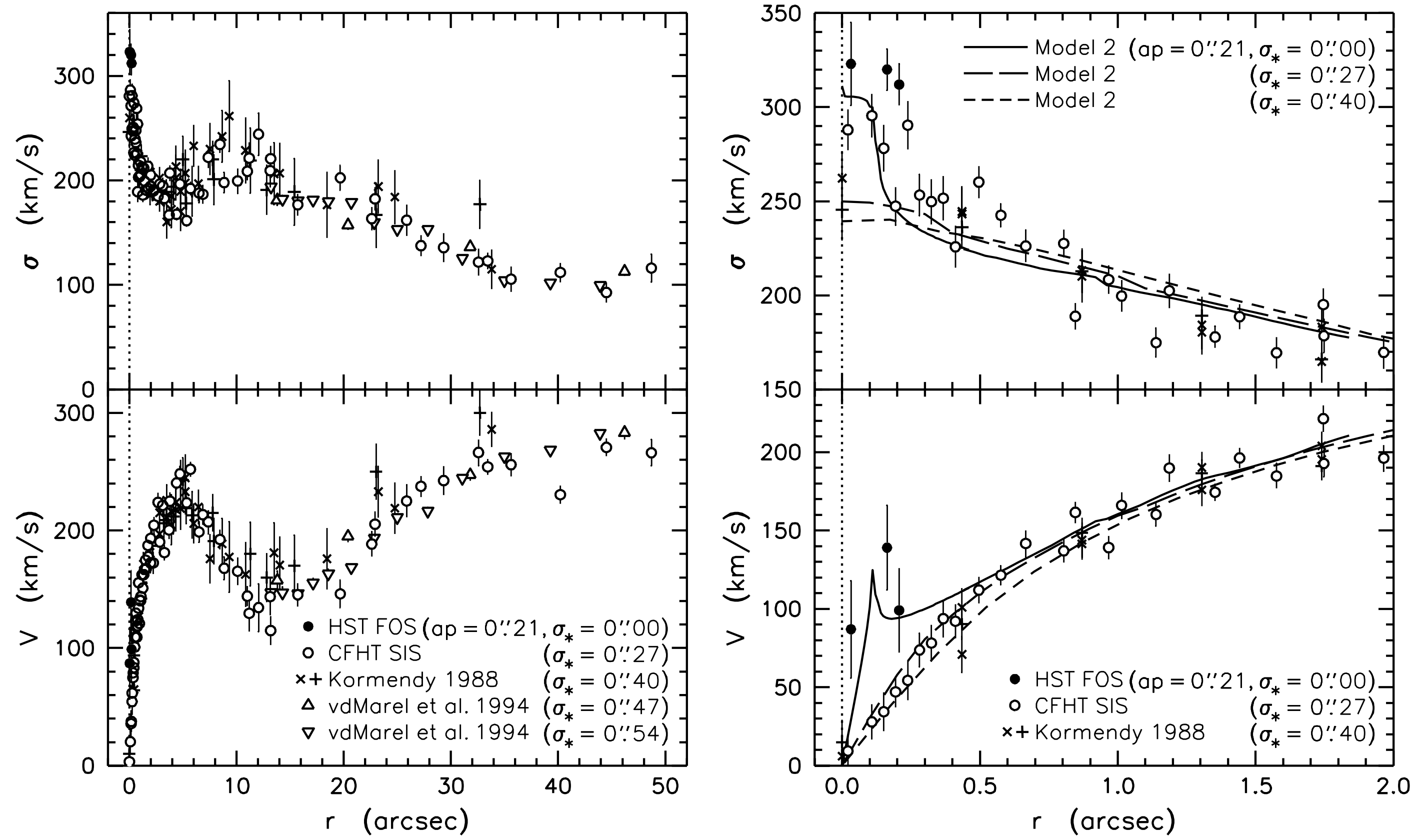

FIG. 2.—Major-axis kinematics of NGC 4594 (*left*) as observed and (*right*) after subtraction of the bulge spectrum. The bulge spectrum was averaged at $|r| = 8'' - 13''$ and shifted to the systemic velocity; neglecting bulge rotation does not affect the results (K88). Bulge subtraction increases V and decreases σ by $\sim$ 25 km s^{-1} at $2''$, but it has essentially no effect near the center, so the *HST* velocities are not bulge-subtracted. The right panel also shows model 2 from K88 as recomputed at SIS and *HST* resolution.

the observed kinematics after projection and seeing convolution; i.e., they provided high- and low-$M_\bullet$ error bars as well as good fits. All models implied that mass-to-light ratios increase rapidly at $r < 1''$ to values $M/L_V > 50$ that are much larger than those of old stellar populations. Two estimates of $M_\bullet$ were derived. If the M/L_V gradient is due to an MDO added to stars with constant $M/L_V(r)$, then $M_\bullet \simeq (1.8 - 4.4) \times 10^9$ M$_\odot$. An alternative estimate is the mass interior to $0\farcs1$: $M_\bullet \simeq (0.4 - 0.8) \times 10^9$ M$_\odot$. K88 concluded that $M_\bullet \simeq 1 \times 10^9$ M$_\odot$, with an estimated error of a factor of 3.

The K88 models were fitted to data with $\sigma_* = 0\farcs40$. We have recomputed them at SIS resolution ($\sigma_* = 0\farcs27$) and FOS resolution ($0\farcs21$ square aperture; $\sigma_* \simeq 0\farcs0$). The result is that all K88 models except number 2 are excluded by the *HST* data. They rotate too slowly near the center, and most do not show the rapid rise in σ at $r < 0\farcs3$. Only the highest-$M_\bullet$ model in K88 approximately fits the *HST* data (Fig. 2, *right*). It has unprojected $\sigma = 265(r/1'')^{-1/2}$ km s^{-1}; $V \simeq 335$ km s^{-1} at large r, changing smoothly to $V = 380(r/1\farcs0)^{-1/2}$ km s^{-1} at $r < 2''$.

Model 2 has only slightly steeper kinematic gradients at $\sigma_* = 0\farcs27$ than at $\sigma_* = 0\farcs40$. It fits the SIS data as it did the K88 data, except that $\sigma(r \leq 0\farcs2)$ is about 40 km s^{-1} higher than predicted. High σ implies a large $M_\bullet$.

Model 2 also is a reasonable description of the *HST* data. At FOS resolution, it shows the rapid rise to $V \simeq 110$ km s^{-1} at $r \simeq 0\farcs14$ and almost the correct high central $\sigma \simeq 321$ km s^{-1} seen in the observations. The reasonable agreement of a high-$M_\bullet$ isotropic model with data taken at resolution 5 times better than the σ_* for which it was derived confirms that the modeling techniques used in past BH papers are reliable (i.e., conservative in their implications about $M_\bullet$). Since only the highest-$M_\bullet$ model is similar to the *HST* data, $M_\bullet$ is larger than K88 derived. On the other hand, we assume a smaller distance (9.2 Mpc versus 18.0 Mpc; see Kormendy & Richstone 1995). Therefore we adopt $M_\bullet = 1 \times 10^9$ M$_\odot$.

One limitation of model 2 deserves discussion. In the 1988 spectra, the sensitivity of the Fourier quotient program to line profile wings was limited by the accuracy of continuum subtraction. Therefore model velocities were restricted to $V \leq 500$ km s^{-1} and $\sigma \leq 300$ km s^{-1}. This does not imply that there are no higher velocity stars; in fact, the *HST* data show that such stars are present. Also, M/L_V already rose by a factor of 4 outside the region where V and σ were set to constant values, so the detection of a dark object was robust. Still, the conclusion that this is a BH and not an extended cluster was less secure than in other galaxies. *HST* now shows steep kinematic gradients, supporting the conclusion that the dark object is a BH.

NGC 4594 is kinematically similar to NGC 3115 (K+96). In NGC 3115, the rotation curve is smoother (there is no dust) and $\sigma(r)$ rises more steeply inside $r = 0\farcs2$. The latter is due to the exceptionally hot stellar nucleus in NGC 3115. This provided a strong and independent argument for an MDO. We do not detect such a nucleus in NGC 4594 (§ 6), so NGC 3115 remains the stronger BH case.

5. EMISSION-LINE KINEMATICS

The detection of emission lines suggests that we try to measure $M_\bullet$ independently of the stellar kinematics. BH detections based on ionized gas velocities have been reported in M 87 (Harms *et al.* 1994) and in NGC 4261 (Ferrarese *et al.* 1996). Unfortunately, gas can also fail to measure masses; NGC 4594 proves to be an example.

Figure 3 shows the emission-line spectrum after a model of the absorption-line spectrum has been subtracted. NGC 4594 is a known mini-Seyfert (Filippenko & Sargent 1985); with our small aperture, dilution by light from the rest of the galaxy is minimal and the broad lines dominate the spectrum. The Hα line has FWZI $\simeq$ 5200 km s^{-1}.

We measured velocities using the narrow lines. This reveals two problems. First, different lines give different velocities (Fig. 3, *bottom*). Most lines agree, but one or two are discrepant, and different lines are discrepant in different apertures. E. g., [OIII] λ 5007 does not agree with the mean of the other lines in the central spectrum, while Hβ does agree; the situation is reversed at $r = -0\overset{''}{.}207$.

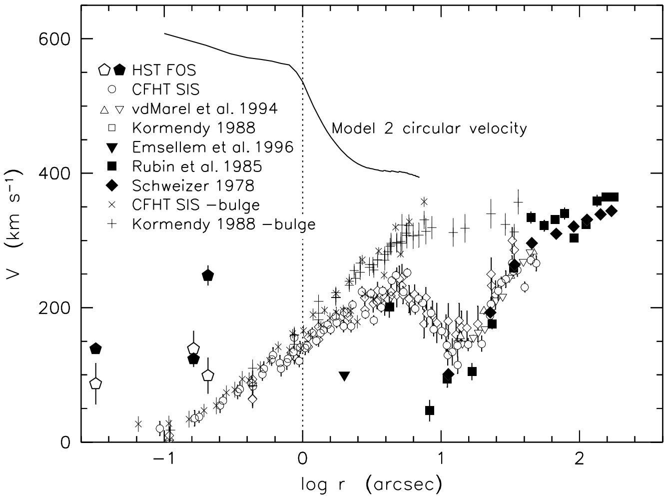

FIG. 4.—Kinematics from emission lines (*filled symbols*) and absorption lines (*open symbols, plus signs, crosses*).

To illustrate the second problem, Figure 4 plots $V(r)$ for the lines that agree with each other. The gas rotates more rapidly in the nuclear disk than at $r \simeq 10''$ (see also Rubin *et al.* 1985). But the gas velocities are much smaller than the circular velocities implied by the stellar dynamics (*solid line*). The same is true at larger radii (Kormendy & Westpfahl 1989; Emsellem *et al.* 1996). In fact, between the nuclear and main disks, the gas velocities are smaller than the stellar velocities. But the latter must be smaller than the circular velocity because the velocity dispersion is large (Fig. 2, *left*; cf. the bulge-subtracted velocities in Fig. 4 ["−bulge"], which have $\sigma \simeq$ 100 km s^{-1} at $r \gtrsim 10''$ and so are closer to circular). Possible reasons are discussed in the above papers; the simplest is that the gas may be in a ring at relatively large radii. The slow rotation is worth further study, but it does mean that the gas velocities do not constrain $M_\bullet$.

6. THE NONTHERMAL NUCLEUS

Figure 1 shows that NGC 4594 has an apparent nucleus. Is this a star cluster or is it a nonthermal source? Absorption-line strengths tell us the answer. Since σ is the same for all three apertures, Figure 1 (*bottom*) shows that the absorption lines look weaker when the nucleus is included. If the true line strengths are the same in all apertures, then the measured equivalent widths of Mg b, Fe λ 5270, and Fe λ 5335 imply that nonthermal flux makes up 50 ± 15 % of the light in the central aperture. This accounts for the extra brightness in the central four pixels (Fig. 1). To check this result, we subtracted the spectrum at $r = 0\overset{''}{.}163$ from that at $r = 0\overset{''}{.}032$. These apertures overlap, but only the latter contains the nucleus. In the difference spectrum, the absorption lines have vanished. This confirms that the central point source is not made of old stars. There is a small possibility that it is made of young, blue stars. But it is more likely to be nonthermal and part of the nuclear activity. The $V - I$ image in Fig. 1 shows that the nucleus is not bluer than the bulge. But there are reddened patches on either side of it, so it may be reddened, too.

We conclude that NGC 4594 is similar to M 87, an active galaxy in which the central point source is nonthermal (Dressler 1989; Dressler & Richstone 1990; Kormendy 1992) and not to M 31 and NGC 3115, which contain nuclear star clusters and apparently quiescent BHs.

We are most grateful to C. D. Keyes, J. Christensen, and J. Hayes for help with the data analysis. This work was supported by HST data analysis funds through grant GO–02600.01–87A and by NSERC. Kormendy's ground-based work was supported by NSF grant AST–9219221. Bender's work was supported by Sonderforschungsbereich 375 of the German Science Foundation and by the Max-Planck-Gesellschaft.

REFERENCES

Bender, R. 1990, A&A, 229, 441
Burkhead, M. S. 1986, AJ, 91, 777
Burkhead, M. S. 1991, AJ, 102, 893
Carter, D., & Jenkins, C. R. 1993, MNRAS, 263, 1049
Dressler, A. 1989, in IAU Symposium 134, Active Galactic Nuclei, ed. D. E. Osterbrock & J. S. Miller (Dordrecht: Kluwer), p. 217
Dressler, A., and Richstone, D. O. 1990, ApJ, 348, 120
Emsellem, E., Monnet, G., Bacon, R., & Nieto, J.-L. 1994, A&A, 285, 739
Emsellem, E., Bacon, R., Monnet, G., & Poulain, P. 1996, A&A, 312, 777
Ferrarese, L., Ford, H. C., & Jaffe, W. 1996, ApJ, 470, 444
Filippenko, A. V., & Sargent, W. L. W. 1985, ApJS, 57, 503
Harms, R. J., *et al.* 1994, ApJ, 435, L35
Jarvis, B. J., & Dubath, P. 1988, A&A, 201, L33
Keyes, C. D., *et al.* 1995, FOS Instrument Handbook (Baltimore: STScI)
Kormendy, J. 1988, ApJ, 335, 40 (K88)
Kormendy, J. 1992, ApJ, 388, L9
Kormendy, J. 1994, in The Nuclei of Normal Galaxies, ed. R. Genzel & A. I. Harris (Dordrecht: Kluwer), p. 379
Kormendy, J., *et al.* 1996, ApJ, 459, L57 (K+96)
Kormendy, J., & Richstone, D. 1992, ApJ, 393, 559
Kormendy, J., & Richstone, D. 1995, ARA&A, 33, 581
Kormendy, J., & Westpfahl, D. J. 1989, ApJ, 338, 752
Morgan, W. W., & Keenan, P. C. 1973, ARA&A, 11, 29
Rubin, V. C., Burstein, D., Ford, W. K., & Thonnard, N. 1985, ApJ, 289, 81
Schweizer, F. 1978, ApJ, 220, 98
van der Marel, R. P., Rix, H.-W., Carter, D., Franx, M., White, S. D. M., & de Zeeuw, T. 1994, MNRAS, 268, 521
Wagner, S. J., Dettmar, R.-J., & Bender, R. 1989, A&A, 215, 243